Microstructure, transport, and acoustic properties of open-cell foam samples

Camille Perrot, Guy Bonnet, M. T. Hoang, F. Chevillotte, F.-X. Bécot, Laurent Gautron, A. Duval

18TH INTERNATIONAL CONGRESS ON SOUND & VIBRATION
ICSV18
RIO DE JANEIRO
BRAZIL
10–14 JULY 2011

MICROSTRUCTURE, TRANSPORT, AND ACOUSTIC PROPERTIES OF REAL FOAM SAMPLES

Camille Perrot, Guy Bonnet, Minh Tan Hoang

Université Paris-Est, Laboratoire Modélisation et Simulation Multi Echelle, MSME UMR 8208 CNRS, 5 bd Descartes, 77454 Marne-la-Vallée, France
e-mail: camille.perrot@univ-paris-est.fr

Fabien Chevillotte, François-Xavier Bécot

Matelys - Acoustique & Vibrations, 1 rue Baumer, 69120 Vaulx-en-Velin, France

Laurent Gautron

Université Paris-Est, Laboratoire Géomatériaux et Environnement, LGE EA 4508, 5 bd Descartes, 77454 Marne-la-Vallée, France

Arnaud Duval

Faurecia Acoustics and Soft Trim Division, R&D Center, Route de Villemontry, Z.I. BP13, 08210 Mouzon, France

This article explores the applicability of numerical homogenization techniques for analyzing transport properties in real foam samples mostly open-cell, to understand long-wavelength acoustics of rigid-frame air-saturated porous media, on the basis of microstructural parameters. Experimental characterization of porosity and permeability of real foam samples are used to provide the scaling of a polyhedral unit-cell. The Stokes, Laplace, and diffusion-controlled reaction equations are numerically solved in such media by a finite element method in three-dimensions; an estimation of the materials' transport parameters is derived from these solution fields. The frequency-dependent visco-inertial and thermal response functions governing the long-wavelength acoustic wave propagation in rigid-frame porous materials are then determined from generic approximate but robust models and compared to standing wave tube measurements. With no adjustable constant, the predicted quantities were found to be in acceptable agreement with multi-scale experimental data, and further analyzed in light of scanning electron micrograph observations and critical path considerations.

1. Introduction

The determination from local scale geometry of the acoustical properties which characterize the macro-behavior of porous media is a long-standing problem of great interest [1], for instance for the oil, automotive, and aeronautic industries. Recently, there has been a great interest in understanding the low Reynolds viscous flow, electrical, and diffusive properties of fluids in the pore structure of real porous media on the basis of microstructural parameters [2], as these transport phe-

nomena control their long-wavelength frequency-dependent properties [3, 4]. Our aim in this paper is to get insight into the microstructure of real porous media and to understand how it collectively dictates their macro-scale acoustic properties, from the implementation of first-principles calculations on a three-dimensional idealized periodic unit-cell.

2. Direct static characterization of foam samples

Three real and commercially available polymeric foam samples have been studied. They are denoted R_1, R_2, and R_3. Real foam samples are disordered and possess a complex internal structure which is difficult to grasp quantitatively. However, our objective is to be able to quantify the local geometry of such foams by an idealized packing of polyhedral Periodic Unit Cells (PUC). Apart from the intrinsic need for characterizing the cell morphology itself, insight into the morphology of an idealized PUC is helpful for understanding the microphysical basis behind transport phenomena. Fig. 1 shows typical micrographs of these real polyurethane foam samples (based on a polyester or polyether polyol), taken with the help of a binocular.

Foam samples were cut perpendicularly to the plane of the sheet. To get an idea of the cellular shape of these samples, the number of edges per face n was measured from 30 different locations for each material. From these measurements follows an average number of edges per face for each foam sample: R_1, $n_1 = 5.10 \pm 0.82$; R_2, $n_2 = 5.04 \pm 0.68$; R_3, $n_3 = 5.03 \pm 0.71$. Next, ligaments lengths were measured on optical micrographs of the foam samples. Since the surface contains exposed cells whose ligament lengths are to be measured on micrographs obtained by light microscopy, great care was taken during measurements to select only ligaments lying in the plane of observation. Ligament length measurements were performed on three perpendicular cross-sections of each sample. Transverse isotropy of the foam samples cellularity was assumed. Here, only results of ligament length measurement distributions on the horizontal surface were plotted in Fig. 2.

Ligament thicknesses constitute also an important geometrical parameter. However, they were difficult to measure. Therefore, the ligament thicknesses were not used. It was observed that computing the permeability of the unit-cell from the averaged ligaments length L_m and open porosity ϕ, produces a significant overestimate of the permeability which results from the exaggerated contribution of the very large cells with atypically high permeability. More precisely, the permeability is related primarily to critical sections and not to mean sections. This argument is supported by critical path considerations. As a consequence, the parameters characterizing the geometry of the PUC are determined in this work from two routinely available measured macroscopic parameters: the porosity ϕ, and the static permeability k_0, which are measured using direct and standard methods. Results are presented in Tab. 1.

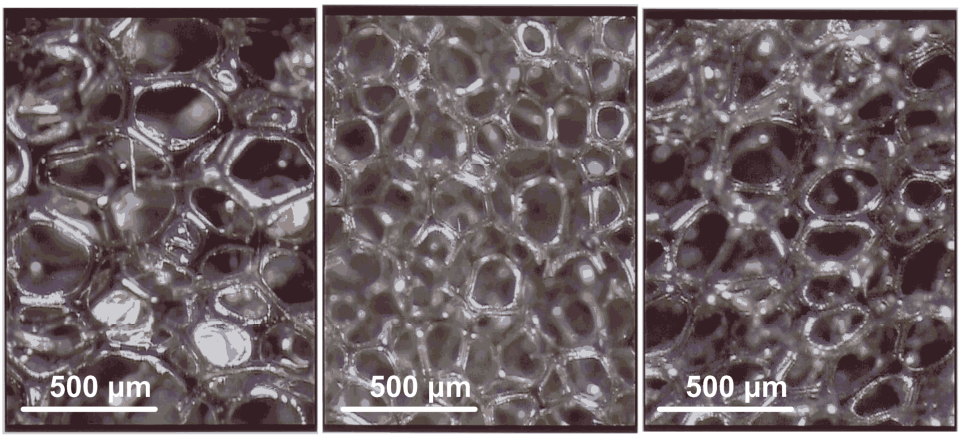

(a) (b) (c)

Fig. 1. Typical micrographs of real foam samples: (a) R_1, (b) R_2, and (c) R_3.

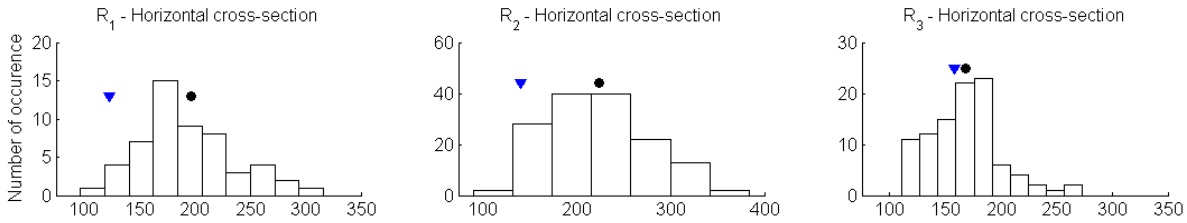

Fig. 2. Ligament length distributions for real foam samples R_1, R_2, and R_3.

3. Prediction of transport properties from a three-dimensional periodic unit-cell

3.1 The local geometry

As observed from the micrographs, the network of ligaments appears to be similar to a lattice within which the ligaments delimit a set of polyhedra. In this work, it is therefore considered that a representation of the microstructure which can be deduced from this observation is a packing of identical polyhedra. More precisely, truncated octahedra with ligaments of circular cross section shapes and a spherical node at their intersections were considered. It has been shown in a recent paper by using 2D computations [4] that the FEM results are not significantly affected by this approximation, even if the real cross-section of ligaments can be rather different.

A regular truncated octahedron is a 14-sided polyhedron (tetrakaidecahedron) having six squares faces and eight hexagonal faces, with ligament lengths L and thicknesses $2r$. The average number of edges per face, another polyhedron shape indicator, is equal to $(6\times4 + 8\times6) / 14 \approx 5.14$ and close to the experimental data presented in Section 2. The cells have a characteristic size D equal to $(2\sqrt{2})L$, between two parallel squared faces. An example of regular truncated octahedron for such packings is given in Fig. 3.

The simplest macroscopic parameter characterizing a porous solid is its open porosity, defined as the fraction of the interconnected pore fluid volume to the total bulk volume of the porous aggregate, ϕ. The porosity of such a packed polyhedron sample might be expressed as a function of the aspect ratio $L/2r$,

$$\phi = 1-\left(3\sqrt{2}\pi/16\right)\left(2r/L\right)^2-\left(\sqrt{2}\pi C_1/16\right)\left(2r/L\right)^3,\quad C_1=-f^3+2(f^2-1)\sqrt{f^2-1}, \qquad (1)$$

and f is a node size parameter related to the spherical radius R by $R = f \times r$, with $f \geq \sqrt{2}$. This last constraint on the node parameter ensures that the node volume is larger than the volume of the connecting ligaments at the node.

Tab. 1. Foam samples macroscopic parameters.

Foams	Method	ϕ (-)	Λ' (μm)	k_0 (m^2)	α_0 (-)	Λ (μm)	α_∞ (-)	k_0' (m^2)	α_0'
R_1	Computations	0.98	506	2.60×10^{-9}	1.22	297	1.02	5.01×10^{-9}	1.13
	Measurements								
	Characterization		440			129	1.12	8.30×10^{-9}	
R_2	Computations	0.97	477	2.98×10^{-9}	1.26	279	1.02	5.85×10^{-9}	1.14
	Measurements								
	Characterization		330			118	1.13	9.70×10^{-9}	
R_3	Computations	0.98	647	4.24×10^{-9}	1.22	373	1.01	8.18×10^{-9}	1.13
	Measurements								
	Characterization		594			226	1.06	13.10×10^{-9}	

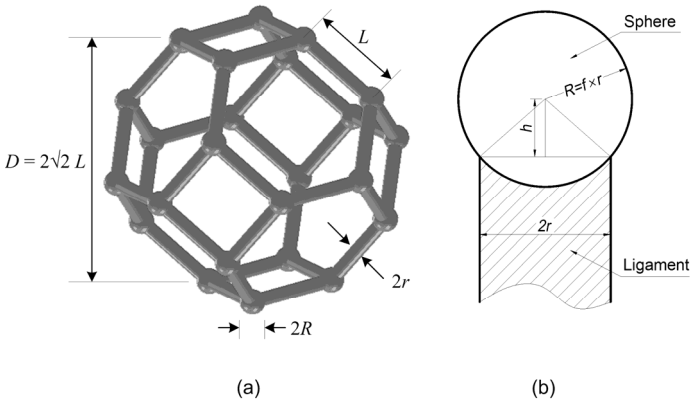

Fig. 3. Basic 3D periodic foam model geometry

The second parameter which is widely used to characterize the macroscopic geometry of porous media, and thus polyhedron packing, is the specific surface area S_p, defined as the total solid surface area per unit volume. The hydraulic radius is defined as twice the ratio of the total pore volume to its surface area. This characteristic length may also be referred to as the "thermal characteristic length" Λ' in the context of sound absorbing materials [1], so that $\Lambda' = 2\phi/S_p$. As for the porosity, the "thermal characteristic length" might be expressed in terms of the microstructural parameters by

$$\Lambda' = \left\{ \left[16\sqrt{2} / \left(\frac{2r}{L} \right)^3 - 6\pi / \left(\frac{2r}{L} \right) - 2\pi C_1 \right] \Big/ \left[3\pi \left(2 / \frac{2r}{L} + C_2 \right) \right] \right\} \times r, \quad C_2 = -f^2 + 2(f-1)\sqrt{f^2-1}. \quad (2)$$

3.2 Determination of the unit cell aspect ratio from porosity

When a laboratory measurement of porosity is available, the unit-cell aspect ratio $L/2r$ can be identified through Eq. (1). For a given value of the spherical node size parameter f, the unit-cell aspect ratio $2r/L$ is given by the solution of a cubic equation that has only one acceptable solution. Once $2r/L$ is obtained, Eq. (2) gives r if a laboratory measurement of S_p is available. Then, the idealized geometry of the foam could be completely defined. The main problem in this method is that the specific surface area evaluation from non-acoustical measurements, such as the standard Brunauer, Emmett, and Teller method (BET) based on surface chemistry principles, is not routinely available. In fact, the most widely measured parameter after the porosity to characterize the physical macro-behavior of real porous media is unarguably the static viscous (or hydraulic) permeability k_0, a quantity having units of a surface (squared length).

Therefore, obtaining the local characteristic sizes of the PUC will be performed thereafter in four steps. Step 1 consists in acquiring the aspect ratio $L/2r$ from the porosity measurements as explained before. For a given spherical node size parameter, this produces all characteristic length ratios of the cell. At this stage, the ligament length of the cell is still unknown, but a non-dimensional PUC can be built. Step 2 is to characterize the permeability of the foam from routine measurements. Step 3 is to get the permeability of the set of non-dimensional periodic cells from first principle calculations. As explained before, the non-dimensional cell has a unit side of square faces. The Finite Element computation described thereafter implemented on the non-dimensional cell produces the non-dimensional permeability k_d. Let D be the side of square faces of homothetic periodic cells producing the static permeability k_0. Then, a simple computation shows that $k_0 = D^2 k_d$. Finally, comparing the non-dimensional permeability to the true permeability produces in step 4 the size of the PUC. All other parameters are obtained from the non-dimensional results through a similar scaling.

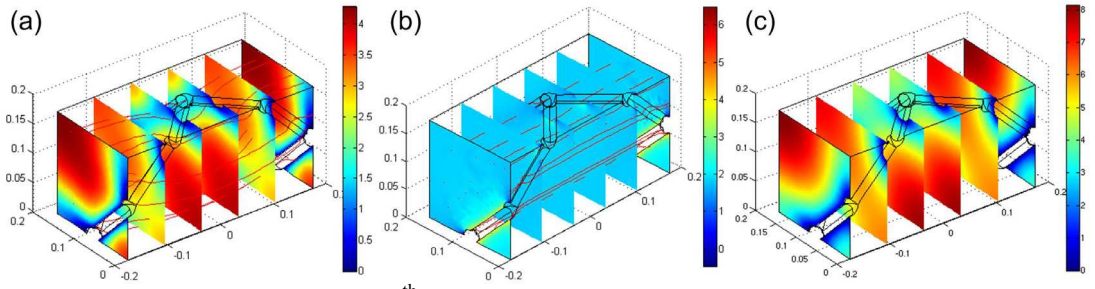

Fig. 4. Asymptotic scaled fields for 1/4th of the reconstructed foam sample period R_1: (a) Stokes velocity field, (b) potential velocity field, and (c) diffusion-controlled concentration field.

3.3 First principles calculations of transport properties

Previous studies [3] have shown how the long-wavelengths acoustic properties of rigid-frame porous media can be numerically determined by solving the local equations governing the asymptotic frequency-dependent visco-thermal dissipation phenomena in a periodic unit cell with the adequate boundary conditions. In the following, it is assumed that $\lambda >> D$, where λ is the wavelength of an incident acoustic plane wave. This means that for characteristic lengths on the order of $D \sim 0.5$ mm, this assumption is valid for frequencies reaching up to a few tens of kHz. The asymptotic macroscopic properties of sound absorbing materials are computed from the numerical solutions of: (1) the low Reynolds number viscous flow equations (the static viscous permeability k_0, and the static viscous tortuosity α_0); (2) the non-viscous flow or inertial equations (the high-frequency tortuosity α_∞, and Johnson's velocity weighted length's parameter Λ); (3) the equations for thermal conduction (the static thermal permeability k_0', and the static thermal tortuosity α_0').

As previously mentioned, all this procedure assumes that the spherical node size parameter f is known. In our computations, f was set to 1.5. This value respects the constraint $f \geq \sqrt{2}$ and is in a rather good agreement with microstructural observations, considering the absence of lump at the intersection between ligaments (see Fig. 1). Application of the above procedure yields the local characteristic sizes of a unit cell ligament for each foam sample: R_1, $L_1 \approx 123.3$ μm, $2r_1 \approx 19.4$ μm; R_2, $L_2 \approx 141.1$ μm, $2r_2 \approx 27.3$ μm; R_3, $L_3 \approx 157.7$ μm, $2r_3 \approx 24.8$ μm.

3.4 Results on asymptotic transport properties obtained from FE modeling

An example of calculated viscous flow velocity, inertial flow velocity, and scaled concentration fields is shown in Fig. 4 for foam sample R_1. The number of elements and their distribution in the fluid phase regions of the PUC were varied, with attention paid especially to the throat and the near-wall areas, to examine the accuracy and convergence of the field solutions. The symmetry properties of the permeability/tortuosity tensors were also checked, as a supplementary test on convergence achievement. As previously noticed by several authors, due to the slip condition, the fluid flow paths are more homogeneous for the electric-current paths than for the viscous fluid flow. Direct numerical computations of the complete set of macroscopic parameters were performed in reconstructed unit cells from adequate asymptotic field averaging. Results are reported in Tab. 1. Some values are compared to estimations obtained from impedance tube measurements.

4. Estimate of the frequency dependent responses by a hybrid numerical approach

The acoustic response of foams depends on dynamic viscous permeability and "dynamic thermal permeability". Both of these parameters could be obtained from dynamic FEM computations. The approach presented here relies on the fact that the finite element computations presented previously are easy to implement and provide the asymptotic behavior for both dynamic "permea-

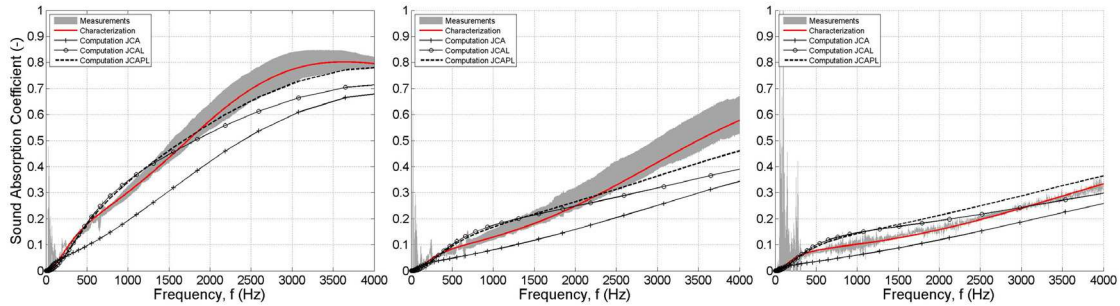

Fig. 5. Normal incidence sound absorption coefficient for foam sample R_1 (left), R_2 (centre), and R_3 (right).

bilities". This asymptotic behavior constitutes the input data for the models which are used for predicting the full frequency range of the dynamic "permeabilities". Therefore the hybrid approach employed in our study makes use of the asymptotic parameters of the porous medium obtained by finite elements. Then, it is possible to provide the dynamic permeabilities and to compare these values to experimental ones. As explicated, the comparison between non-dimensional permeability obtained from finite element results and the measured permeability provides the thermal characteristic length Λ'; and five remaining input parameters for the models, α_0, α_∞, Λ, k_0', and α_0' are obtained by means of first-principles calculations by appropriate field-averaging in the PUC [3]. Finally, we considered the predictions of the three models for the effective dynamic permeabilities. In summary, the Johnson-Champoux-Allard" [JCA] model which uses the 5 parameters (ϕ, k_0, α_∞, Λ, Λ') , Johnson-Champoux-Allard-Lafarge" model [JCAL] which uses in addition k_0', and Johnson-Champoux-Allard-Pride-Lafarge" [JCAPL] model which uses the full set of parameters (ϕ, k_0, k_0', α_∞, Λ, Λ', α_0, and α_0').

5. Assessment of the methodology through experimental results

5.1 Experimental results and comparison with numerical results

One main objective of this section is to produce a comparison between sound absorption coefficients coming from experimental results using the impedance tube technique by Utsuno *et al.* [5], and from numerical computations. In this context, intermediate results were obtained for the acoustic parameters of the JCAL model through the characterization method described in Refs. 6 for viscous and thermal dissipations. These results will be thereafter referenced to on the Figs. and Tab. as obtained from "characterization".

Fig. 5 produces the sound absorption coefficient obtained from measurements, from characterization and from numerical computations. Despite the simplicity of the local geometry model used to study the multi-scale acoustic properties of real foam samples predominantly open-cell, there is a relatively good agreement between computed (present microstructural method), measured (impedance tube measurements), and characterized quantities. The general trend given in term of normal incidence sound absorption coefficient $A_n(\omega)$ by our microstructural approach appears as being particularly relevant, if we notice that it requires only ϕ and k_0, as input parameters, and proceeds without any adjustable parameter.

Discrepancies between measured and computed sound absorption coefficient at normal incidence can be primarily explained from the comparison of a set of parameters obtained from numerical results and from the characterization method reported in Tab. 1; namely Λ', Λ, α_∞, and k_0'. From that comparison, it can be seen that the most significant difference is the large overestimation provided for Λ. This means that, at high frequencies, the windows size of the local geometry model, which respectively plays the role of weighting the velocity field for Λ and rapid section changing for α_∞ by their small openings (the squares in the case of a truncated octahedron unit-cell), is presumably overestimated by a monodisperse, isotropic, and membrane-free local geometry model.

Consequently, an improvement of the local geometry model would result in the introduction of a second set of characteristic sizes. The purpose of the following is to examine more thoroughly the microstructure in order to provide some means aimed at improving the methodology.

5.2 Keys for further improvements of the methodology

A supplementary visual cell inspection is given by electron micrographs at very low magnification, as presented in Fig. 6. The characteristic ligament length L_c obtained for the periodic cell is reported on the micrographs, which allows a first visual comparison between observed and computed cell size. Another element of discussion is provided in Fig. 2 where the distribution of the measured ligament lengths is reported (together with its mean value L_m), simultaneously with the length L_c obtained from the numerical results and from the calibration coming from (k_0, ϕ). The characteristic ligament length L_c of the local geometry model provides a basis for understanding the influence of certain local geometry features, such as membrane effects and cell anisotropy, on the static viscous permeability of the real foam samples – in connection with ligaments length distribution.

More precisely, if the distribution of the ligament lengths is sharply peaked, one would expect the overall system behavior to be similar to that of the individual elements. This is a configuration close to the one observed for foam sample R_3, where only isolated residual membranes (thermal reticulation process) and no specific cell elongation were observed, as illustrated on the electron micrograph in Fig. 6(c); and for which the distribution of the ligaments length is relatively sharp. As a result, the ligaments length of the local geometry model for foam sample R_3 is relatively close to the averaged value measured on the micrographs, especially for the horizontal surface through which permeability measurements were performed ($L_c \approx 158$ µm, $L_{m3H} \approx 167$ µm, and $L_{m3H} / L_c \approx 1.06$).

On the other hand, if the distribution is broader as shown for foam sample R_2 in Fig. 2, because of cell elongation as it can be seen on Fig. 6 (b), the critical path - made by the small windows at the openings of the cells - is expected to dominate (in Fig. 2, for the horizontal surface $L_{m2H} \approx 227$ µm, whereas $L_c \approx 141$ µm, and L_{m2H} / L_c is now equal to 1.61).

Similarly, as observed for foam sample R_1 in Fig. 6(a), the presence of membranes occludes or significantly reduces the size of some windows which might belong to unit-cells in the class of local permeability sites k_{ij} (in the sense of critical path considerations) much greater, or of the order of k_c. This has in addition the effect of disconnecting some critical subnetworks. In this later case, the unit-cells which were belonging to the permeability sites with $k_{ij} \leq k_c$, may now significantly contribute by participating in a new critical subnetwork, lowering drastically k_c (in Fig. 2, for the horizontal surface, $L_{m1H} \approx 193$ µm, whereas $L_c = 123$ µm, and L_{m1H} / L_c gives 1.57).

As explained before, reporting the value of L_c on the electron micrograph of Fig. 6 can illustrate what is the typical size of a critical path opening. It is also worth mentioning that L_c and $D_c = (2\sqrt{2})L_c$ provide a rather reliable rough estimate of the characterized values for Λ and Λ' respectively. This tends to confirm the customarily assumed idea that the small openings (windows) and the pore itself (cell) are respectively associated to viscous and thermal dissipation effects.

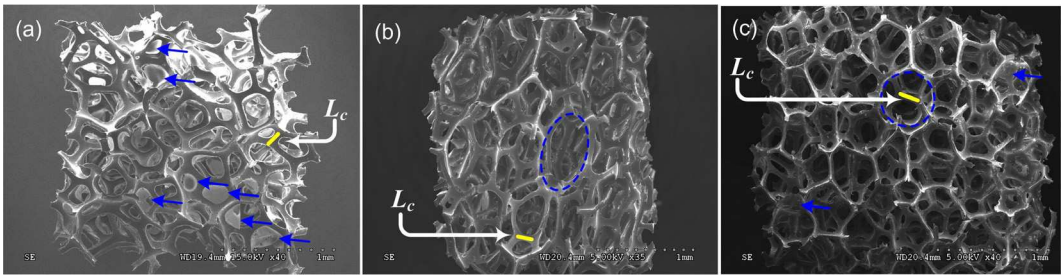

Fig. 6. Typical SEM images of real foam samples. (a) R_1, showing a relatively great number of membranes (indicated by arrows). (b) R_2, having a degree of anisotropy equal to 1.75 (superimposed ellipse). (c) R_3, exhibits only few isolated membranes with rather spherical pore shapes.

6. Conclusion

A three-dimensional idealized periodic unit-cell (PUC) based method to obtain the acoustic properties of three predominantly open-cell foam samples was described. The first step was to provide the local characteristic lengths of the representative unit cell. For isotropic open cell foams, two input parameters were required, the porosity and the static viscous (hydraulic) permeability. Long-wavelengths acoustic properties were derived from the three-dimensional reconstructed PUC by solving the boundary value problems governing the micro-scale propagation and visco-thermal dissipation phenomena with adequate periodic boundary conditions, and further field phase averaging. The computed acoustic properties of the foams were found to be in relatively good agreement with standing wave tube measurements. A close examination of the real foam sample ligament length distribution as observed from micrographs, and its comparison with the characteristic size of the local geometry model, showed evidences of membrane and cellular anisotropy effects discussed by means of critical path considerations. In summary, we have developed a microcellular approach in which the local characteristic length L_c governing the static viscous permeability of a real foam sample can be identified; and from which rough estimates of the viscous Λ and thermal lengths Λ' may follow (small openings and pore size itself). The overall picture that emerges from that work is that the acoustical response of these materials is governed by their three-dimensional micro-cellular morphology, for which an idealized unit-cell based method is a convenient framework of multi-scale analysis displaying the microgeometry features having a significant impact on the overall response function of the porous media.

Acknowledgments

This work was part of a project supported by ANRT and Faurecia Acoustics and Soft Trim Division under convention CIFRE No. 748/2009.

REFERENCES

[1] J. F. Allard and N. Atalla, *Propagation of Sound in Porous Media: modeling sound absorbing materials*, 2nd Ed. (Wiley, Chichester, 2009).

[2] P. M. Adler, *Porous Media: Geometry and Transports* (Butterworth-Heinemann, Stoneham, 1992).

[3] D. Lafarge, The equivalent fluid model (Chapter 6, Part II) in *Materials and Acoustics Handbook*, Edited by C. Potel and M. Bruneau (Wiley, Chichester, 2009) pp 167-201.

[4] C. Perrot, F. Chevillotte, and R. Panneton, "Bottom-up approach for microstructure optimization of sound absorbing materials", *J. Acoust. Soc. Am.* **124**, 940 (2008).

[5] H. Utsuno, T. Tanaka, T. Fujikawa, A. F. Seybert, "Transfer function method for measuring characteristic impedance and propagation constant of porous materials", *J. Acoust. Soc. Am.* **86**, 637 (1989).

[6] R. Panneton, X. Olny, "Acoustical determination of the parameters governing viscous dissipation in porous media", *J. Acoust. Soc. Am.* **119**, 2027 (2006); X. Olny, R. Panneton, "Acoustical determination of the parameters governing thermal dissipation in porous media", *J. Acoust. Soc. Am.* **123**, 814 (2008).